A convolution model for computing the far-field directivity of a parametric loudspeaker array

Chuang Shi[a)] and Yoshinobu Kajikawa

Department of Electrical and Electronic Engineering

Kansai University

3-3-35 Yamatecho, Suita, Osaka Prefecture, Japan 564-8680

[a)]e-mail: r148005@kansai-u.ac.jp

Abstract

This paper describes a method to compute the far-field directivity of a parametric loudspeaker array (PLA), whereby the steerable parametric loudspeaker can be implemented when phased array techniques are applied. The convolution of the product directivity and the Westervelt's directivity is suggested, substituting for the past practice of using the product directivity only. Computed directivity of a PLA using the proposed convolution model achieves significant improvement in agreement to measured directivity at a negligible computational cost.

I. INTRODUCTION

The parametric loudspeaker is an application of the parametric acoustic array in air[1;2]. It allows an equally narrow audio beam to be created from a significantly smaller aperture size compared to the conventional loudspeaker and loudspeaker array. Past studies of the parametric loudspeaker focused mostly on suppressing the harmonic distortion[3;4;5] and improving the sound quality[6]. In those studies, the ultrasonic emitter of the parametric loudspeaker was assumed to be a circular or rectangular source, even though it was made up of numerous piezoelectric ultrasonic transducers (PZTs) in practice. If the PZTs could be grouped into several channels and fed different driving signals, the overall system becomes a parametric loudspeaker array (PLA), since each channel in such a system is effectively a parametric loudspeaker. It has been proven by experiments that the delay-and-sum beamforming approach applied to the primary waves can control the directivity of the difference frequency wave in a PLA[7;8].

However, there is difficulty in computing the far-field directivity of a PLA, especially when the computational power is constrained. In Westervelt's original derivation[1], the directivity of the difference frequency wave was described by the Westervelt's directivity under assumptions that the primary waves were transmitted in collimated narrow beams and the resultant difference frequency wave would propagate like a linear wave. Since then, Berktay has extended Westervelt's derivation in two aspects[9]. Firstly, an envelope function

is introduced to describe the self-demodulation process of a pulsed ultrasonic carrier on its propagation axis. This leads to the Berktay's far-field solution, which is the most widely applied model equation in past studies of the parametric loudspeaker[4;5;6]. Secondly, an aperture factor is considered to compensate for the discrepancy between measured directivity and the Westervelt's directivity. The aperture factor is a function of the wavenumber of the difference frequency wave depending on the shape of the ultrasonic emitter.

Following that, Berktay and Leah developed Berktay's extensions and included the product directivity of the primary waves in a volume integral to amend the computed far-field directivity of a parametric transmitting array[10]. In other words, the aperture factor has been substituted by the product directivity of the primary waves. They have further interpreted that when the product directivity of the primary waves is as sharp as an impulse function, the volume integral is simplified into the Westervelt's directivity; and when the Westervelt's directivity is as sharp as an impulse function, the volume integral is simplified into the product directivity. All aforementioned model equations comply with the assumption of collimated narrow beams. Hence, none of them can be readily applied to a PLA. With the exception of main lobes, side lobes and grating lobes of the primary waves are rarely collimated in a PLA[8]. Furthermore, the directivity of a PLA is usually of interest within an angular range implied by the beam width of the PZTs. For example,

some PZTs resonating at 40 kHz with a diameter of 10 mm possess a typical beam width of 80°. Therefore, the directivity of a PLA made up of these PZTs should be measured from −40° to 40° with respect to the normal axis of the PZTs. This wide angular range conflicts with the assumption of narrow beams of the primary waves.

On the other hand, the Khokhlov–Zabolotskaya–Kuznetsov (KZK) equation describes the combined nonlinear effects of absorption, diffraction, and nonlinearity, which is not strictly restricted by the assumption of collimated narrow beams[11]. Due to the parabolic approximation, the KZK equation is applicable in the paraxial region, which has an approximate angular validity limit of $\pm 20°$[12]. This is not wide enough for many applications of the parametric acoustic array. Hence, several researchers have attempted to extend the applicability of the KZK equation to arbitrary angles. For example, Fox *et al.* have substituted the steered beam axis for the normal axis of the ultrasonic emitter to become the propagation axis so that the KZK equation can be used to compute steered nonlinear fields[13]. Kamakura *et al.* have used two Padé terms in the analysis of the nonlinear propagation of a parametric sound beam emitted from a circular piston source, and excellent agreement between measured directivity and computed directivity using their proposed model equation has been achieved[14]. A combination of these two mentioned approaches would lead to a viable numerical solution to the far-field directivity of a PLA, if the computational cost was not a constrain.

Therefore, previous attempts to compute the far-field directivity of a PLA simply uses the product directivity of the primary waves, which is inspired by Darvennes and Hamilton's seminal work on the intersection of two Gaussian beams[15]. Despite its ease of application, the accuracy of the product directivity model is adequately good, only in the vicinity of grating lobes of the primary waves[8]. A modification to the product directivity model, namely the advanced product directivity model, has been previously proposed[16]. Improved agreement between measured directivity and computed directivity has been observed particularly at directions near the first side lobes of the primary waves. However, overall accuracies of both product directivity models are not yet satisfactory. This is probably because the equivalent transformation from a linear array of piston sources to a circular array of Gaussian sources is carried out based on directivity matching. Hence, a PLA consisting of 8 channels is approximated only by 7 Gaussian sources at the frequency of each primary wave. As compared to the classic Gaussian source expansion of a piston source[17], there are 10 Gaussian sources to represent a piston source accurately. Hence, a possibility of improving the product directivity models is through finding an accurate Gaussian source expansion of a PLA, but once again this brings up the issue of computational complexity.

In this paper, a convolution model to compute the far-field directivity of a PLA is derived from the Westervelt's directivity. The convolution model is a simple analytical

equation and gives accurate predictions of the far-field directivity of a PLA when different

phased array techniques are applied. Moreover, the convolution model is also able to be

applied to a parametric loudspeaker, as the parametric loudspeaker is an unsteered PLA

when a common driving signal is fed to all channels with no delays. The applicability of

the convolution model to the curved and omnidirectional PLAs[18;19] is expected but beyond

the discussion of this paper.

II. THEORY

A. Westervelt's Directivity

Assumptions made in Westervelt's treatment are invoked[1]. The primary waves are

transmitted in extremely narrow and perfectly collimated beams, so that the volume

distribution of virtual sources of the secondary waves is represented adequately by a line

distribution along the propagation direction of the primary waves. The pressure level of

the primary sound field at a distance x and time t is considered in the form of

$$p_i\left(x\right) = \sum_{n=1}^{2} P_n e^{-\alpha_n x} \cos\left(\omega_n t - k_n x\right), \tag{1}$$

where P_n, α_n and k_n are the amplitude, attenuation rate, and wavenumber of the primary

wave at ω_n respectively.

The geometry in Fig. 1 is adopted to derive the Westervelt's directivity. The

ultrasonic emitter is placed at the origin and the observation point is located at a distance
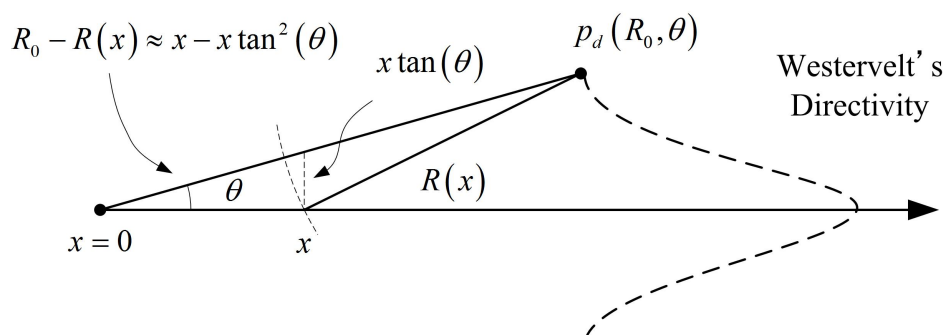
$$R_0 - R(x) \approx x - x\tan^2(\theta) \qquad x\tan(\theta) \qquad p_d(R_0, \theta)$$

Westervelt's
Directivity

θ

$R(x)$

$x = 0$

x

Figure 1: Geometry of the Westervelt's directivity.

of R_0 and an off-axis angle of θ. Nonlinear interactions between the primary waves create

virtual sources along the x axis. Westervelt has derived the source strength density of the

secondary waves as

$$q = \frac{\beta}{\rho_0^2 c_0^4} \frac{\partial}{\partial t} p_i^2, \tag{2}$$

where β and ρ_0 are the nonlinear coefficient and density of a homogeneous and viscous

medium respectively; c_0 is the speed of sound at infinitesimal amplitude in the medium[1].

For parametric loudspeakers, air is assumed to be the homogeneous and viscous medium.

Inserting Eq. (1) into Eq. (2) yields a decomposition into three terms as

$$q = q_h + q_s + q_d. \tag{3}$$

The first term on the right side of Eq. (3) is the source strength density of the harmonic

waves, which is given by

$$q_h = \frac{\beta}{\rho_0^2 c_0^4} \sum_{n=1}^{2} \omega_n P_n^2 e^{-2\alpha_n x} \sin\left(2k_n x - 2\omega_n t\right). \tag{4}$$

The second term is the source strength density of the sum frequency wave, which is given

by

$$q_s = \frac{\beta}{\rho_0^2 c_0^4} \omega_s P_1 P_2 e^{-\alpha_s x} \sin\left(k_s x - \omega_s t\right), \tag{5}$$

where $\alpha_s = \alpha_1 + \alpha_2$ is defined; $\omega_s = \omega_1 + \omega_2$ and $k_s = k_1 + k_2$ are the angular frequency and

wavenumber of the sum frequency wave respectively.

The third term on the right side of Eq. (3) is of the most interest to a PLA as well as

a parametric loudspeaker. It is the source strength density of the difference frequency

wave, which is given by

$$q_d = \frac{\beta}{\rho_0^2 c_0^4} \omega_d P_1 P_2 e^{-\alpha_s x} \sin\left(k_d x - \omega_d t\right), \tag{6}$$

where $\omega_d = |\omega_1 - \omega_2|$ and $k_d = |k_1 - k_2|$ are the angular frequency and wavenumber of the

difference frequency wave. For simplicity, Eq. (6) is rewritten as the real component of a

complex source strength density:

$$q_d = \frac{\beta}{2\rho_0^2 c_0^4} \omega_d P_1 P_2 e^{-\alpha_s x} \times \left(-j e^{jk_d x - j\omega_d t}\right) + c.c., \tag{7}$$

where j is the imaginary unit and *c.c.* is short for complex conjugate.

The far-field pressure level of the difference frequency wave can be obtained from the volume integral, which is given by

$$p_d = \frac{\rho_0}{4\pi} \int \int \int \frac{\partial q_d}{\partial t} \frac{e^{j\omega_d R(x,y,z)}}{R(x,y,z)} dxdydz, \tag{8}$$

where $R(x, y, z)$ is the distance from the observation point to a virtual source. Berktay and Leah have multiplied the product directivity with the integral kernel[10] and numerical techniques are requested to solve this volume integral and its variants[20;21;22]. Noting that the volume distribution of virtual sources of the difference frequency wave is represented adequately by the line distribution give by Eq. (7), the far-field pressure level of the difference frequency wave is simplified into the linear integral, which is given by

$$p_d(R_0, \theta) = \frac{\rho_0 S_0}{4\pi} \int_0^l \frac{\partial q_d}{\partial t} \frac{e^{jk_d R(x)}}{R(x)} dx, \tag{9}$$

where S_0 is the cross-sectional area of collimated beams; l is the length of the virtual source array; $R(x)$ is the distance from the observation point to a virtual source locating at x.

Under the far-field and absorption-limited source conditions[1;21], l should be much shorter than R_0 and yet long enough so that the primary waves are sufficiently attenuated beyond the point $x = l$. Therefore, $R(x)$ can be approximated by R_0 in the denominator and by $R_0 - x + x \tan^2 \theta$ in the exponent of the Green's function in Eq. (9). Applying these approximations and inserting Eq. (7) into Eq. (9) yield

$$p_d(R_0, \theta) = \frac{-\beta \omega_d^2 P_1 P_2 S_0}{8\pi \rho_0 c_0^4 R_0} e^{jk_d R_0 - j\omega_d t} \int_0^l e^{-\alpha_s x + jk_d x \tan^2 \theta} dx + c.c.. \tag{10}$$

This linear integral in Eq. (10) is elementary. When the primary waves are transmitted in perfectly collimated beams, we can change the upper limit of the integral from l to $+\infty$ without introducing much error. However, this approximation leads to a larger computed pressure level if the primary waves are not transmitted in well collimated beams. Nonetheless, by changing the upper limit of the integral to $+\infty$, we obtain

$$p_d\left(R_0, \theta\right) = \frac{\beta \omega_d^2 P_1 P_2 S_0}{8\pi \rho_0 c_0^4 R_0} \frac{e^{jk_d R_0 - j\omega_d t}}{-\alpha_s + jk_d \tan^2 \theta} + c.c. \tag{11}$$

and rewrite it as

$$p_d\left(\theta\right) = K P_1 P_2 D_W\left(\theta\right)\cos\left(\omega_d t - k_d R_0 - \phi\right), \tag{12}$$

where

$$K = -\frac{\beta \omega_d^2}{4\pi \alpha_s R_0 \rho_0 c_0^4}; \tag{13}$$

$$D_W\left(\theta\right) = \frac{\alpha_s}{\sqrt{\alpha_s^2 + k_d^2 \tan^4 \theta}} \tag{14}$$

is the Westervelt's directivity; and

$$\tan \phi = \frac{k_d \tan^2 \theta}{\alpha_s} \tag{15}$$

is the angular response.

B. Convolution Model

Eq. (12) can be further modified for collimated beams of the primary waves transmitted at an off-axis angle of ψ_n in stead of $0°$ in the previous subsection. Pressure
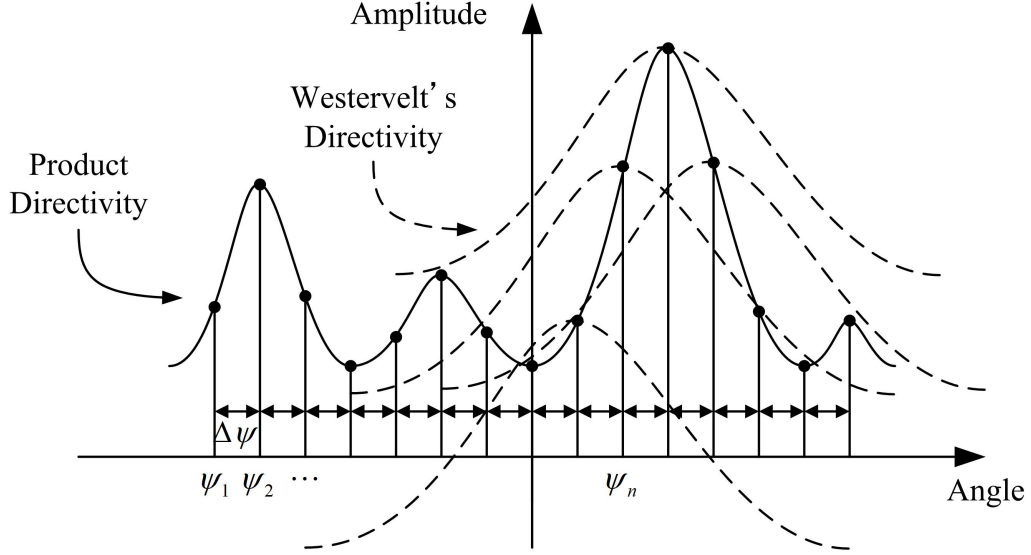
Figure 2: Geometry of the convolution model for computing the far-field directivity of a parametric loudspeaker array.

levels of the primary waves are expressed by $P_1 = D_1(\psi_n)$ and $P_2 = D_2(\psi_n)$, where $D_1(\theta)$ and $D_2(\theta)$ are two real functions of the angular variable θ. At this step, it is assumed that $D_1(\theta)$ and $D_2(\theta)$ have non-zero values only at $\theta = \psi_n$. Therefore, the pressure level of the difference frequency wave in the far field is given by

$$p_d(\theta) = K D_1(\psi_n) D_2(\psi_n) D_W(\theta - \psi_n) \cos(\omega_d t - k_d R_0 - \phi_n),\tag{16}$$

where the angular response is modified to

$$\tan\phi_n = \frac{k_d \tan^2(\theta - \psi_n)}{\alpha_s}.\tag{17}$$

Assuming that only weak nonlinear interactions occur in a PLA, the wave superposition principle is still valid for the difference frequency wave. When more than one pair of collimated beams of the primary waves are transmitted in a space, the pressure level of the difference frequency wave can be presented in a summation as

$$p_d\left(\theta\right) = K \sum_{n=1}^{N} D_1\left(\psi_n\right) D_2\left(\psi_n\right) D_W\left(\theta - \psi_n\right) \cos\left(\omega_d t - k_d R_0 - \phi_n\right). \tag{18}$$

where N is the total number of collimated beam directions; $D_1\left(\theta\right)$ and $D_2\left(\theta\right)$ become discrete functions representing directivity of the primary waves. When $N = 1$ and $\theta_1 = 0$, Eq. (18) is simplified back to Eq. (12).

Substituting $\psi_n = \left(n - \frac{N+1}{2}\right)\Delta\psi$ into Eq. (18) and dropping the angular response term, we obtain

$$p_d\left(\theta\right) = K \cos\left(\omega_d t - k_d R_0\right) \sum_{n=-\frac{N-1}{2}}^{\frac{N-1}{2}} D_1\left(n\Delta\psi\right) D_2\left(n\Delta\psi\right) D_W\left(\theta - n\Delta\psi\right). \tag{19}$$

When $\Delta\psi$ is approaching infinitesimal, Eq. (19) is rewritten in the integral form as

$$p_d\left(\theta\right) = K \cos\left(\omega_d t - k_d R_0\right) \int_{-\psi_0}^{\psi_0} D_1\left(\psi\right) D_2\left(\psi\right) D_W\left(\theta - \psi\right) d\psi, \tag{20}$$

where ψ_0 is the upper angular limit of the computed directivity of the difference frequency wave.

Eq. (20) complies with the definition of convolution. When the directivity of the primary waves in a PLA are denoted as $D_1\left(\theta\right)$ and $D_2\left(\theta\right)$, the directivity of the difference

frequency wave is computed using Eq. (20) as

$$D_d\left(\theta\right) = \left[D_1\left(\theta\right) D_2\left(\theta\right)\right] \otimes D_W\left(\theta\right), \tag{21}$$

where $\otimes$ denotes the linear convolution operation.

Hence, the directivity of the difference frequency wave is given by the convolution of the product directivity and the Westervelt's directivity. As aforementioned, Berktay and Leahy have observed in their proposed volume integral that when the product directivity is as sharp as an impulse function, the volume integral is simplified into the Westervelt's directivity; and when the Westervelt's directivity is as sharp as an impulse function, the volume integral is simplified into the product directivity[10]. The same observation is made by the convolution model as well. In digital signal processing, the linear convolution operation is the fundamental of digital filters. The Westervelt's directivity serves as a spatial filter on the product directivity of the primary waves. When the Westervelt's directivity is as sharp as an impulse function, the directivity of a PLA becomes a sampled version of the product directivity. When the Westervelt's directivity is wide, the directivity of a PLA is given by a smoothed version of the product directivity. Therefore, side lobes are not likely to be observed in the PLA.

III. RESULTS
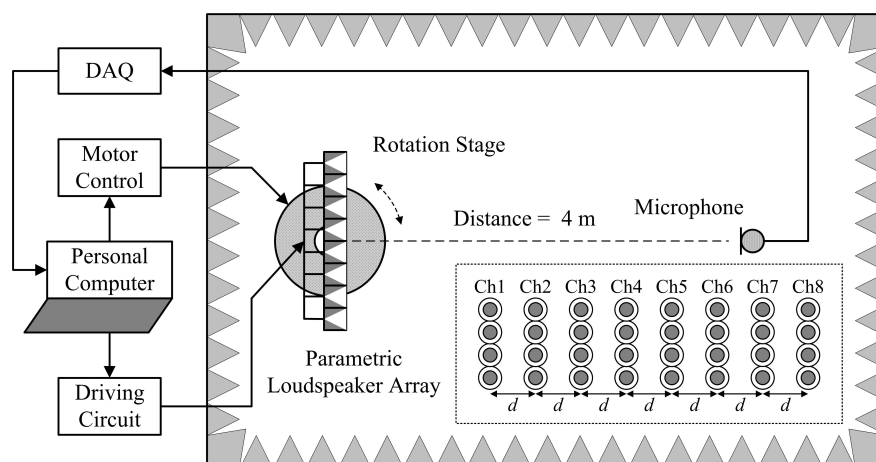
A. Measurement Setup

Figure 3: Measurement setup of a laboratory-made parametric loudspeaker array.

The measurement setup of a laboratory-made PLA is illustrated in Fig. 3. The PLA consists of 8 channels and every channel consists of 4 PZTs. The uniform spacing between channels is adjustable. A bi-frequency ultrasonic signal is fed to all channels, but it is delayed by different amounts in every channel in order to steer the primary waves to a desired direction. All PZTs have a resonance frequency of about 40 kHz and a diameter of 9.9 mm. The typical beam width of the PZTs is 80°. When driven at the resonance frequency, the PLA is capable of transmitting a maximum pressure level of 120 dB measured at 4 m away from the PLA.

Measurements are carried out in an anechoic chamber with a dimension of $6\,(m) \times 3\,(m) \times 3\,(m)$. Room temperature is maintained at 20°C, but relative humidity

varies. Directivity of the PLA is measured from $-40°$ to $40°$ at a resolution of $1°$ controlled by a rotation stage. The primary and difference frequency waves are captured by B&K Type 4138 and 4134 microphones respectively. The microphones are placed at a distance of 4 m away from the center of the rotation stage, which is considered to be the far field of the PLA and the primary waves have been sufficiently attenuated.

Directivity and frequency response of the PZTs have already contributed to measured directivity of the primary waves. Therefore, when directivity of the difference frequency wave is computed using measured directivity of the primary waves, the convolution model and product directivity models can be compared with reference to measured directivity of the difference frequency wave. In figures of the following subsections, measured directivity of the difference frequency wave is labeled as "Measurement"; product directivity of the primary waves is labeled as "Product Directivity"; the computed directivity using the convolution model is labeled as "Convolution"; the computed directivity using the advanced product directivity model is labeled as "Gaussian Directivity", since measured directivity of the primary waves is approximated by a circular array of Gaussian sources in the first step of this method[16].

B. Collimated Main Lobes of the Unsteered Primary Waves

First of all, an unsteered PLA is tested. Room temperature and relative humidity are
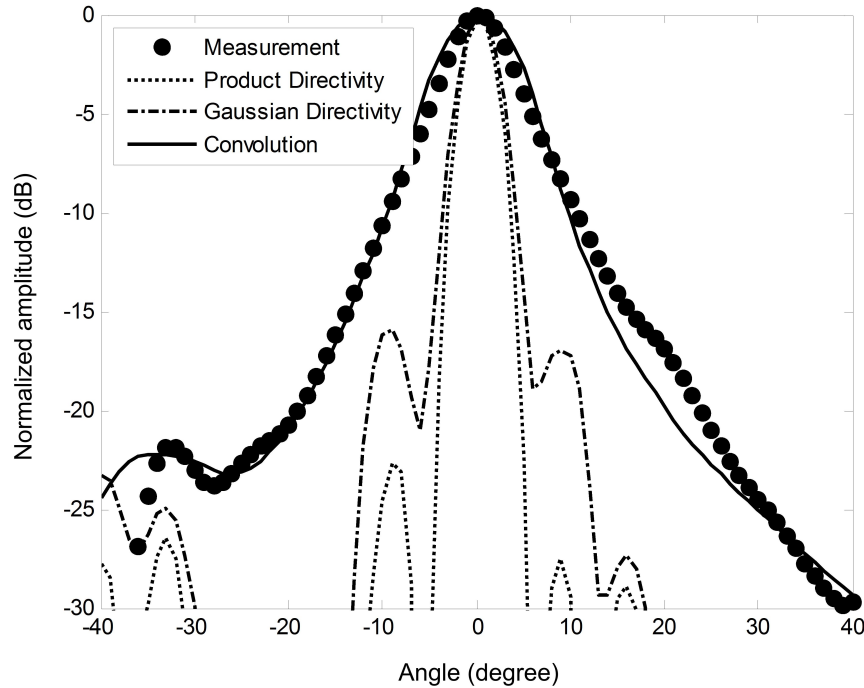
Figure 4: Directivity of the difference frequency wave at 4 kHz generated from the primary waves at 38 kHz and 42 kHz.

recorded at 20°C and 30% respectively. The bi-frequency ultrasonic signal is generated as a combination of 38 kHz and 42 kHz sine waves. The uniform spacing between channels is set to 10 mm. Since no delay is implemented, this unsteered PLA functions identically to a parametric loudspeaker. Maximum pressure levels of the primary waves at 38 kHz and 42 kHz are recorded as 103.7 dB and 109.7 dB respectively. The difference frequency wave is created at 4 kHz by the parametric acoustic array in air. The maximum pressure level of
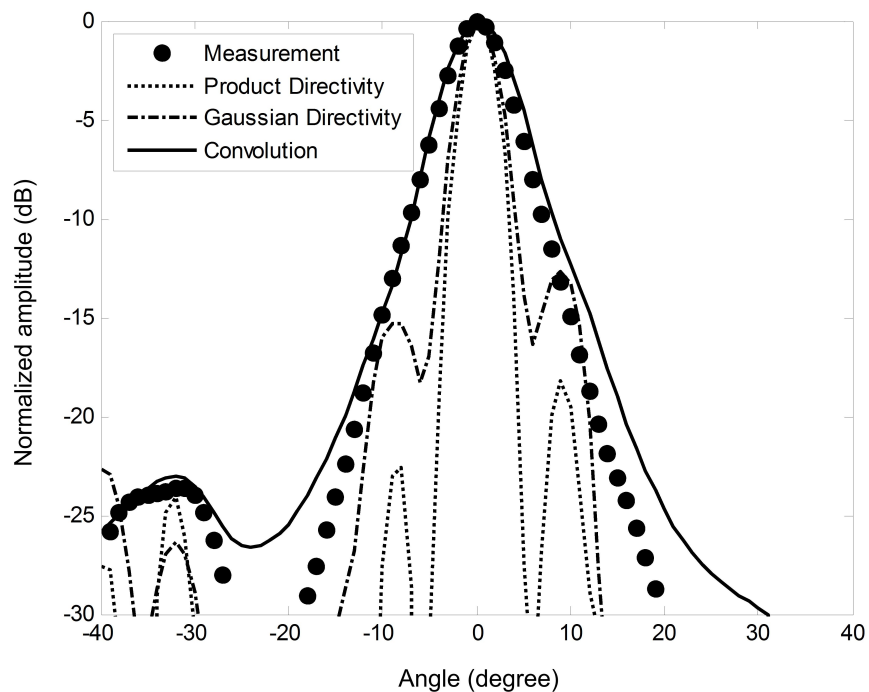
Figure 5: Directivity of the difference frequency wave at 8 kHz generated from the primary waves at 36 kHz and 44 kHz.

the 4 kHz wave is recorded as 54.0 dB.

Measured directivity and computed directivity are normalized and plotted in Fig. 4. The proposed convolution model shows the best results among the three directivity models. It provides us with the closest matches to the measured directivity at angles from $-30°$ to $40°$. The product directivity models fail to match the beam width of the difference frequency wave. Their predictions tend to provide a much narrower main lobe and a few

side lobes that are not observed in the measured directivity. Some mismatches of the computed directivity using the convolution model to the measured directivity are observed only from $-40°$ to $-30°$. However, none of the three directivity models shows good agreement in this angular range.

In addition, it is known from the Nyquist-Shannon sampling theorem that a maximum spacing of 4.1 mm is necessary to avoid spatial aliasing of the primary wave at 42 kHZ. Undoubtedly, grating lobes are observed in the measured directivity of the primary waves. However, they are not found in the measured directivity of the difference frequency wave as shown in Fig. 4. This is explained by grating lobe elimination[8]. Because spatial aliasing period depends on frequency, the primary waves at different frequencies have different spatial aliasing periods. When main lobes of the primary waves are collimated, their grating lobes are separated and result in eliminated grating lobes of the difference frequency. Grating lobe elimination becomes obvious when the ratio of the difference frequency to the higher primary frequency or carrier frequency is sufficiently large. For example, in a parametric loudspeaker using a carrier frequency of 40 kHz, grating lobe elimination is generally observed when the difference frequency is above 2 kHz.

Next, the bi-frequency ultrasonic signal is changed to a combination of 36 kHz and 44 kHz sine waves. Maximum pressure levels of the primary waves at 36 kHz and 44 kHz are recorded as 95.5 dB and 103.0 dB respectively. The difference frequency wave at 8 kHz

achieves a maximum pressure level of 50.7 dB. Because grating lobe elimination occurs, there is no grating lobe but a small side lobe of the difference frequency wave observed in Fig. 5.

The results from the proposed convolution model is still the best among the three directivity models. Close matches to the measured directivity are observed in vicinities of the main lobe ranging from $-20°$ to $20°$ and the side lobe ranging from $-40°$ to $-30°$. The advanced product directivity model outperforms the product directivity. However, both product directivity models are not able to match the measured directivity closely. Mismatches of the computed directivity using the convolution model to the measured directivity are observed at angles from $-30°$ to $-20°$ and from $20°$ to $40°$. At these angles, the primary waves are not strong enough to generate a long virtual source array. As discussed after Eq. (10), when the length of the virtual source array is not long enough, the approximation of making $l = +\infty$ causes a larger computed pressure level than the measured value. Despite all these factors, the proposed convolution model is able to predict the beam width and side lobe attenuation accurately for the unsteered PLA in our measurements.

C. Collimated Main Lobes of the Steered Primary Waves

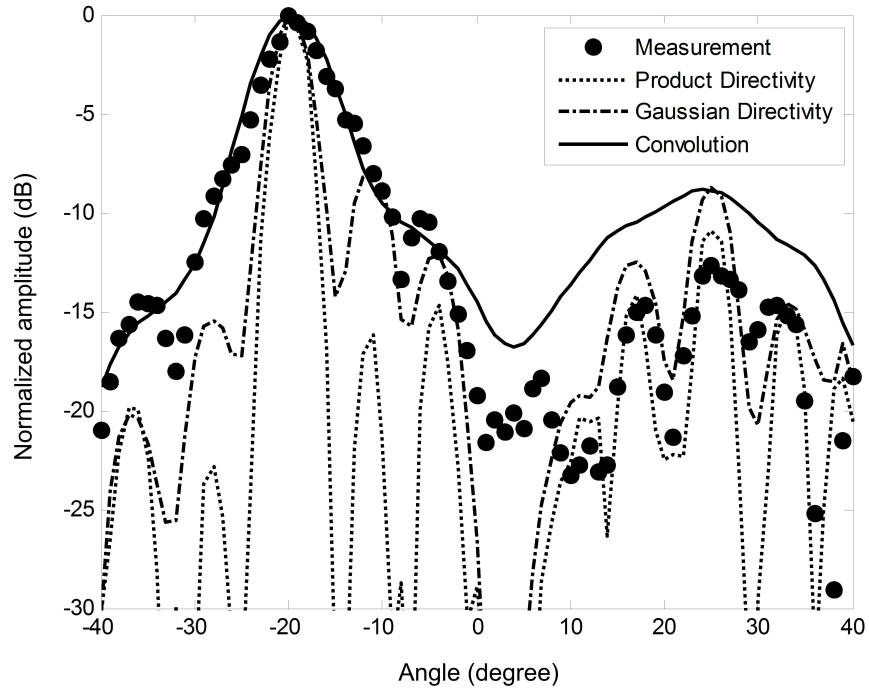In the case of a steered PLA, the uniform spacing between channels remains at 10

Figure 6: Directivity of the difference frequency wave at 4 kHz steered to −20° from the primary waves at 38 kHz and 42 kHz.

mm. Room temperature and relative humidity are recorded at 20°C and 50% respectively. The bi-frequency ultrasonic signal is generated as a combination of 38 kHz and 42 kHz sine waves. A delay line is implemented in every channel to steer main lobes of the primary waves simultaneously to −20°. The primary waves at 38 kHz and 42 kHz achieve maximum pressure levels of 101.3 dB and 101.4 dB respectively. The readings are lower than those in the unsteered PLA due to directivity of the PZTs. The difference frequency wave at 4 kHz

achieves a maximum pressure level of 49.7 dB.

Measured directivity and computed directivity are normalized to this pressure level and plotted in Fig. 6. The proposed convolution model predicts the most accurate main lobe as compared to the product directivity models. However, an almost constant error of 3 dB is observed in the vicinity of the side lobe. This can be explained by the approximation of making $l = +\infty$ in Eq. (10). After compensating for the 3dB error, the convolution model still cannot match the notches closely in the measured directivity. However, the product directivity model is uncannily accurate in this angular range. It shows that the actual Westervelt's directivity becomes much sharper than the theoretical one given by Eq. (14) in the vicinity of the side lobe. As compared to the product directivity model, the advanced product directivity improves agreement to the measured directivity at first side lobes of the primary waves, but introduces errors at the side lobe of the difference frequency wave. Overall, the trade off is between predicting the main lobe and matching the side lobe. Therefore, the convolution model, which is able to yield the most accurate beam width, is of the great importance to applications of the PLA.

The bi-frequency ultrasonic signal is changed to a combination of 36 kHz and 44 kHz sine waves. Both the primary waves at 36 kHz and 44 kHz are steered to $-20°$. Maximum pressure levels of the primary waves at 36 kHz and 44 kHz are recorded as 90.8 dB and 94.8 dB respectively. The difference frequency wave at 8 kHz achieves a maximum pressure
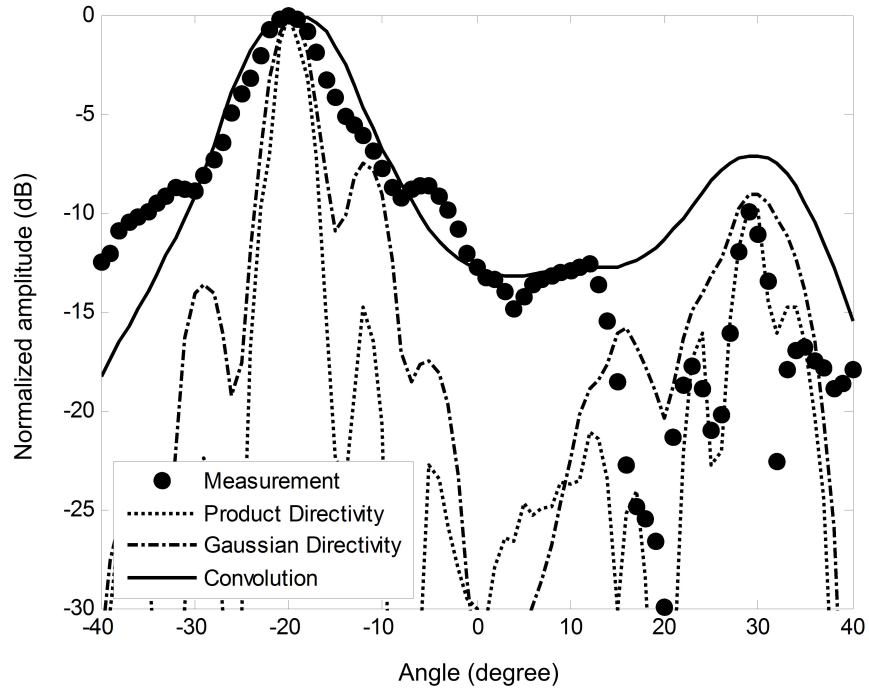
Figure 7: Directivity of the difference frequency wave at 8 kHz steered to $-20°$ from the primary waves at 36 kHz and 44 kHz.

level of 45.6 dB. Similar discrepancies are observed in Fig. 7. There is a trade off between the agreement to the main lobe and the side lobe. The convolution model is better at predicting the main lobe of the difference frequency wave, but the product directivity model works excellently for matching the side lobe in the measured directivity. Once again, the convolution model predicts a higher side lobe than the measured directivity. The applicability of the convolution model to uncollimated beams of the primary waves at large

intersection angles may be limited, while the product directivity model is well suited for these exceptional cases.

D. Uncollimated Main Lobes of the Primary Waves

In this subsection, the convolution model is demonstrated when a dedicated beamforming approach enabling a PLA to transmit two sound beams simultaneously is adopted[23]. In this beamforming approach, different delay lines are implemented in every channel for the primary waves. Therefore, main lobes of the primary waves are steered to different directions on purpose. As aforementioned, the primary waves at different frequencies have different spatial aliasing periods. When main lobes of the primary waves are collimated, grating lobes are separated by the difference in their spatial aliasing periods leading to grating lobe elimination[8]. However, if the main lobes are steered to different directions that are separated by half of the difference in spatial aliasing periods, the grating lobes will be separated by the same amount. In this case, one sound beam of the difference frequency wave is resulted from nonlinear interactions of the main lobes, and another sound beam is resulted from the grating lobes of the primary waves. Therefore, this beamforming approach is called the dual beam generation. Without any changes to the hardware configuration of a PLA, the confined sound can be shared into another location. Potential applications of the dual beam generation can be found in spatial audio and assistive listening[24], where more than one steerable parametric loudspeakers using the
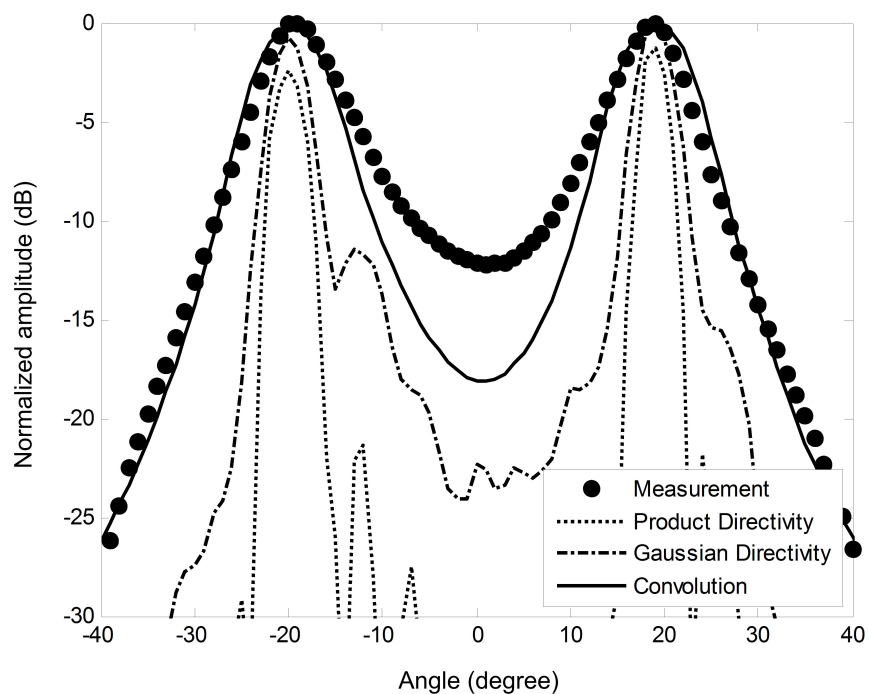
Figure 8: Directivity of the difference frequency wave at 4 kHz steered to $\pm 20°$ from the primary waves at 38 kHz and 42 kHz.

same carrier frequency interfere with each other. Using the dual beam generation, we are able to explore the performance of the convolution model for uncollimated main lobes of the primary waves.

Room temperature and relative humidity are recorded at 20°C and 20% respectively. In order to generate dual beams of the difference frequency wave at $\pm 20°$, the uniform spacing between channels is adjusted to 12.5 mm. Different delay lines are implemented in
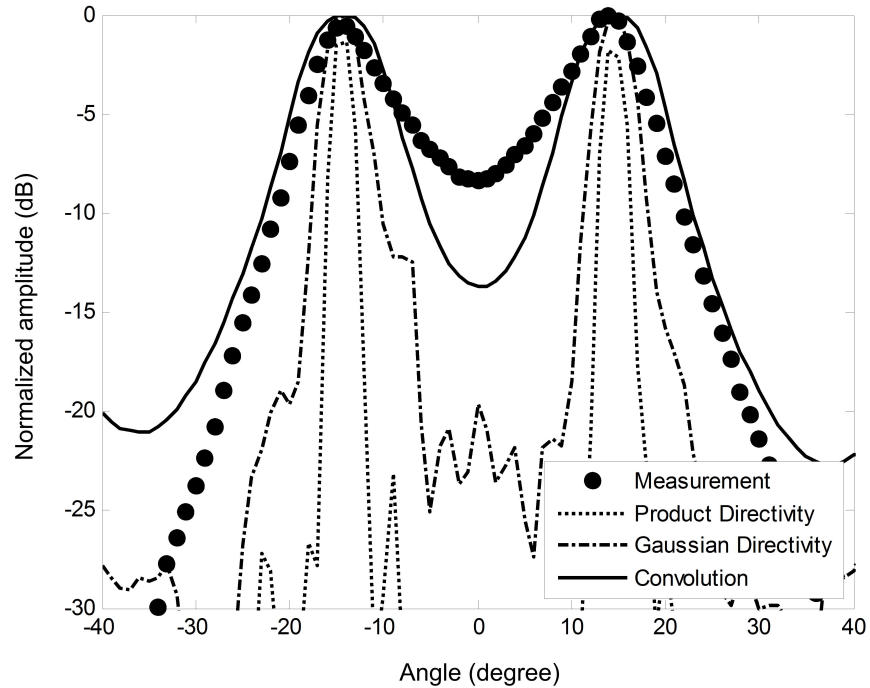
Figure 9: Directivity of the difference frequency wave at 4 kHz steered to $\pm 15°$ from the primary waves at 42 kHz and 46 kHz.

every channel for the primary waves. The primary waves at 38 kHz and 42 kHz are steered to $-21°$ and $-19°$ and achieve maximum pressure levels of 100.7 dB and 104.4 dB respectively. Grating lobes of the primary waves are found at $21°$ and $19°$ respectively. The resultant difference frequency wave at 4 kHz have two symmetric beams at nearly $\pm 20°$ with a maximum pressure level of 51.3 dB as shown in Fig. 8. As compared to the case of collimated main lobes of the primary waves, the maximum pressure level of the difference

frequency wave is slightly reduced. It is observed in Fig. 8 that the convolution model shows the greatest accuracy among the three directivity models. The agreement of the convolution model to the measured directivity confirms that it is applicable to uncollimated main lobes of the primary waves, as well as grating lobes, but only a small angular separation is allowed.

The uniform spacing between channels is further adjusted to 15 mm to generate dual beams of the difference frequency wave at $\pm 15°$. The primary waves at 42 kHz and 46 kHz are steered to $-15°$ and $-13°$ and achieve maximum pressure levels of 105.0 dB and 93.0 dB respectively. Grating lobes of the primary waves are found at $15°$ and $13°$ respectively. The resultant difference frequency wave at 4 kHz have two symmetric beams at nearly $\pm 15°$ with a maximum pressure level of 41.5 dB as shown in Fig. 9. With combined effects of the frequency response of the PZTs and uncollimated main lobes of the primary waves, this maximum pressure level of the difference frequency wave is much reduced. The convolution model is still by far the most efficient directivity model in this comparison. Mismatches of the computed directivity using convolution model to the measured directivity are found at angles between the dual beams of the difference frequency wave in both Figs. 8 and 9. The discrepancies allows for future improvement on the convolution model.

IV. CONCLUSIONS

This paper has presented an analytical model for computing the far-field directivity of a PLA. Following assumptions made by Westervelt[1] and wave superposition principle, a convolution model has been obtained to represent the far-field directivity of the difference frequency wave in a simple and clear expression. It has been validated by experiments that the convolution model results in excellent to satisfactory matches to measured directivity of a PLA applying different phased array techniques. In conclusion, this concise yet accurate convolution model is recommended in sound field control applications of the PLA. Using the product directivity model as a complement to predict the side lobe attenuation may be necessary when grating lobes of the primary waves are separated by a large angle.

Acknowledgements

REFERENCES

1. P. J. Westervelt, "Parametric acoustic array," *J. Acoust. Soc. Am.* **35**, 535-537 (1963).

2. M. B. Bennett and D. T. Blackstock, "Parametric array in air," *J. Acoust. Soc. Am.* **57**, 562–568 (1975).

3. M. Yoneyama, J. Fujimoto, Y. Kawamo, and S. Sasabe, "The audio spotlight: An

application of nonlinear interaction of sound waves to a new type of loudspeaker design," *J. Acoust. Soc. Am.* **73**, 1013–1020 (1983).

4. T. Kamakura, M. Yoneyama, and K. Ikegaya, "Developments of parametric loudspeaker for practical use," *Proc. 10th Int. Symp. Nonlinear Acoust.*, Kobe, Japan, 147–150 (1984).

5. T. D. Kite, J. T. Post, and M. F. Hamilton, "Parametric array in air distortion reduction by preprocessing," *J. Acoust. Soc. Am.* **103**, 2871 (1998).

6. C. Shi, H. Mu, and W. S. Gan, "A psychoacoustical preprocessing technique for virtual bass enhancement of the parametric loudspeaker," *Proc. 38th Int. Conf. Acoust. Speech Sig. Process.*, Vancouver, Canada, 31–35 (2013).

7. N. Tanaka and M. Tanaka, "Active noise control using a steerable parametric array loudspeaker," *J. Acoust. Soc. Am.* **127**, 3526–3537 (2010).

8. C. Shi and W. S. Gan, "Grating lobe elimination in steerable parametric loudspeaker," *IEEE Trans. Ultrason. Ferroelectrics Freq. Control* **58**, 437-450 (2011).

9. H. O. Berktay, "Possible exploitation of non-linear acoustics in under-water transmitting applications," *J. Sound Vib.* **2**, 435-461 (1965).

10.   H. O. Berktay and D. J. Leahy, "Farfield performance of parametric transmitters," *J. Acoust. Soc. Am.* **55**, 539-546 (1974).

11.   M. F. Hamilton, "Sound beams," in *Nonlinear Acoustics*, edited by M. F.Hamilton and D. T. Blackstock (Academic, San Diego, 1998), Chap. 8, pp. 233-261.

12.   T. Kamakura, T. Ishiwata, and K. Matsuda, "Model equation for strongly focused finite-amplitude sound beams," *J. Acoust. Soc. Am.* **107**, 3035–3046 (2000).

13.   P. D. Fox, A. Bouakaz, and F. Tranquart, "Computation of steered nonlinear fields using offset KZK axes," *Proc. 2005 IEEE Ultrason. Symp.*, Rotterdam, Netherlands, 1984-1987 (2005).

14.   T. Kamakura, H. Nomura, and G. T. Clement, "Application of the split-step Pad e approach to nonlinear field predictions," *Ultrason.*, **53**, 432–438 (2013).

15.   C. M. Darvennes and M. F. Hamilton, "Scattering of sound by sound from two Gaussian beams," *J. Acoust. Soc. Am.* **87**, 1955-1964 (1990).

16.   C. Shi and W. S. Gan, "Product directivity models for parametric loudspeakers," *J. Acoust. Soc. Am.* **131**, 1938-1945 (2012).

17.   J. J. Wen and M. A. Breazeale, "A diffraction beamfield expressed as the superposition of Gaussian beams," *J. Acoust. Soc. Am.* **83**, 1752-1756 (1988).

18. N. Tanaka and M. Tanaka, "Mathematically trivial control of sound using a parametric beam focusing source," *J. Acoust. Soc. Am.* **129**, 165–172 (2011).

19. U. Sayin, P. Artis, and O. Guasch, "Realization of an omnidirectional source of sound using parametric loudspeakers," *J. Acoust. Soc. Am.* **134**, 1899–1907 (2013).

20. T. G. Muir and J. G. Willette, "Parametric acoustic transmitting arrays," *J. Acoust. Soc. Am.* **52**, 1481–1486 (1972).

21. M. B. Moffett and R. H. Mellen, "Model for parametric acoustic sources," *J. Acoust. Soc. Am.* **61**, 325–337 (1977).

22. M. Zheng and L. S. Wang, "The angular response of parametric arrays: General numerical solution," *J. Sound Vib.* **228**, 177–197 (1999).

23. C. Shi, H. Nomura, T. Kamakura, and W. S. Gan, "Spatial aliasing effects in a steerable parametric loudspeaker for stereophonic sound reproduction," *IEICE Trans. Fund. Electron. Comm. Comput. Sci.* .textbfE97A, 1859–1866 (2014).

24. C. Shi, E. L. Tan, and W. S. Gan, "Hybrid immersive three dimensional sound reproduction system with steerable parametric loudspeakers," *POMA* **19**, 055003 (2013).

Figure Captions

Figure 1. Geometry of the Westervelt's directivity.

Figure 2. Geometry of the convolution model for computing the far-field directivity of a parametric loudspeaker array.

Figure 3. Measurement setup of a laboratory-made parametric loudspeaker array.

Figure 4. Directivity of the difference frequency wave at 4 kHz generated from the primary waves at 38 kHz and 42 kHz.

Figure 5. Directivity of the difference frequency wave at 8 kHz generated from the primary waves at 36 kHz and 44 kHz.

Figure 6. Directivity of the difference frequency wave at 4 kHz steered to $-20°$ from the primary waves at 38 kHz and 42 kHz .

Figure 7. Directivity of the difference frequency wave at 8 kHz steered to $-20°$ from the primary waves at 36 kHz and 44 kHz.

Figure 8. Directivity of the difference frequency wave at 4 kHz steered to $\pm20°$ from the primary waves at 38 kHz and 42 kHz.

Figure 9. Directivity of the difference frequency wave at 4 kHz steered to $\pm15°$ from the primary waves at 42 kHz and 46 kHz.